Stable hydrosols for TiO_2 coatings

Pierre Alphonse · Aneesha Varghese · Claire Tendero

Abstract The optimum processing parameters required to synthesize, by hydrolysis of titanium isopropoxide (TIP), highly stable hydrosols composed of nanoparticles of the smallest possible size, are deduced both from data available in literature and from our own experiments. The colloids prepared in these conditions are composed of aggregates of anatase (~90%) and brookite crystallites (5–6 nm). They are suitable for coatings and have long-term stability (more than one year) in terms of polymorphic composition, crystallite and agglomerate size. Stable sols composed solely of anatase crystallites (4 nm) can be prepared by partially complexing the TIP by acetylacetone before hydrolysis. It is not possible to produce porous films with these colloids because they are stabilized by electrostatic repulsion which causes the particles to organize themselves, during the drying step, to form materials with a close packed structure. However, coatings with controlled porosity can be prepared from these stable sols through the post addition of polymers, like PEG or block copolymers.

Keywords Sol–gel · Titanium dioxide · Colloid stability · Porosity · Rheology · Coating

P. Alphonse (✉)
Université de Toulouse, CIRIMAT UPS-CNRS,
118 route de Narbonne, 31062 Toulouse cedex 9, France
e-mail: alphonse@chimie.ups-tlse.fr
URL: http://www.cirimat.cnrs.fr/

A. Varghese · C. Tendero
Université de Toulouse, CIRIMAT INP-CNRS,
118 route de Narbonne, 31062 Toulouse cedex 9, France
e-mail: varghese@chimie.ups-tlse.fr

C. Tendero
e-mail: claire.tendero@ensiacet.fr

1 Introduction

Titania coatings with high specific surface area and tailored pore size have potential applications in fields such as solar energy conversion [1], photocatalysis [2–6] and catalytic supports [7–10]. The pore size and the specific surface area greatly impact the physical properties of these materials and can play a relevant role in their activity. For instance, catalytic applications require a tunable porosity to optimize the diffusion rate of reactants towards the adsorption sites and a high surface area to maximize the interface between the reactant flow and the catalyst surface.

Titania coatings may be synthesized by several methods, but the sol–gel process is ubiquitous because it has many advantages such as purity, homogeneity, control over the microstructure, ease of processing, low temperature, low cost, and the ability to coat large and complex substrates.

The synthesis of titanium dioxide coatings by sol–gel process is typically achieved by the hydrolysis of titanium alkoxide precursors. However, two different routes can be distinguished according to the processing parameters. By far the most common [11–20] is the polymeric route, where the solvent is most often an alcohol and the hydrolysis is carefully controlled by using a limited amount of water. Typically, an acid catalyst (HCl or HNO_3) is added and the alkoxide is complexed prior to hydrolysis thereby decreasing the reaction rate. The shape and size of the polymeric structural units are determined by the relative rate constants of the hydrolysis and polycondensation reactions. This method leads to amorphous films which need to be heat treated to turn crystalline.

In the second route the solvent is water which is in large excess with respect to the alkoxide. In these conditions hydrolysis is very fast producing ultrafine primary particles whose size ranges from 2 to 8 nm [21]. These nanoparticles

agglomerate very rapidly, giving large aggregates of macroscopic dimensions [22]. Peptization by means of an inorganic acid (HCl or HNO_3) is used to break down the aggregates and produce a colloidal suspension containing particles whose size ranges from 15 to 100 nm. At this point, the nanoparticles are crystalline and predominantly anatase with 10–30% of brookite [23]. This second route uses a cheap and non toxic solvent (water) and gives crystalline films with potential applications for coating low thermal stability substrates (polymers). It is this route which was explored in this work.

Most of the sols used in the reported procedures have shown very limited stability (<24 h). It should be emphasized that, for a large scale production of titania coatings (for example, by roll-coating), a long term stability of the titania sol is needed in order to achieve an acceptable repeatability. Actually, among the vast number of works dealing with titania synthesis by sol–gel process, very few were interested in the long term stability of nanoparticles dispersion in water. Thus, the goal of this study was to find the relevant processing parameters required to easily prepare highly stable titania hydrosols suitable for coatings. From the numerous data available in literature and from our own experiments we will first investigate the effect of the main synthesis parameters on the size, the organization and the stability of titania hydrosols. Then we will deduce the optimum processing parameters required to prepare highly stable sols composed of nanoparticles of the smallest possible size. In a second step we will see how the assembling of these nanoparticles can be controlled in order to obtain the required properties, i.e. surface area, porosity, thermal stability, etc.

2 Materials and methods

2.1 Sol synthesis

Titania sols were prepared by hydrolysis of titanium alkoxide in a large excess of acidified water. In a standard procedure titanium (IV) isopropoxide (TIP) previously dissolved in anhydrous isopropyl alcohol (C_3H_8O/Ti = 3.5) was added quickly, under vigorous stirring, to hot (70 °C) water (H_2O/Ti ≈ 90) acidified with nitric acid (H^+/Ti = 0.2). A white precipitate was obtained and the mixture was stirred for 16 h at 80 °C. The white suspension changed gradually, to a translucent sol, by peptization. During the first 6 h the reaction flask was kept uncovered in order to allow the isopropyl alcohol to evaporate (the boiling point of the azeotrope isopropanol-water −87.4–12.6% is 80.3 °C). At the end of peptization the pH of the sol was about 1.4 and the molar concentration of Ti was in the range of 0.6–0.65 M. This is close to the expected concentration if the isopropyl alcohol had totally evaporated (0.62 M). In the following text these synthesis conditions are referred to as "standard".

In some syntheses TIP was used pure without prior dilution in isopropyl alcohol. In others TIP was partially complexed by acetylacetone (acacH/Ti = 0.5) before hydrolysis. Sols containing polymer (PEG2000 or Pluronic™ F127) were prepared by direct addition of the polymer powder into the sol followed by gentle stirring overnight at room temperature.

2.2 Rheology

Rheology measurements on the sols were performed with a rheometer Anton Paar Physica MCR fitted with a cone and plate device. The dimensions corresponding to the geometry were 50 mm for the diameter and 1 ° for the angle. The minimum distance between the plate and truncated cone was 0.05 mm. Rheograms were recorded at 20 °C, over a range of 1–1,000 s^{-1}, with a total time period of 300 s for both the increasing- and decreasing-shear-rate sweeps. For each sample, a minimum of three measurements was performed. Frequently, at lower shear rates (<10 s^{-1}) some fluctuations in viscosity were observed, especially in the case of the less viscous sols.

2.3 Zeta potential and particle hydrodynamic diameter

Electrophoretic mobility and particle hydrodynamic diameters were determined on a Malvern Zetasizer 3000 using a He–Ne laser as the light source ($\lambda = 633$ nm). The zeta potential was calculated from the electrophoretic mobility using the Henry equation and the Smoluchowski approximation.

Samples were prepared by diluting the sols with acidified water (HNO_3). The initial pH was close to 2.0. It was then increased to the required value by addition of NaOH. No electrolyte was added and as a result the ionic strength varied with pH.

Particle sizes were measured by photon correlation spectroscopy (PCS). All size measurements were conducted at 25 °C with a scattering angle of 90 °. To control the effect of multiple scattering and particle interaction, analyses were performed at several dilutions in order to check that the measured size was independent of the dilution.

2.4 Powder X-ray diffraction (PXRD)

The crystal structure was investigated by powder X-ray diffraction. Data was collected, at room temperature, with a Bruker AXS D4 θ–2θ diffractometer, in the Bragg–Brentano geometry, using filtered Cu Kα radiation and a graphite

secondary-beam monochromator. Diffraction intensities were measured by scanning from 20 to 80 ° (2θ) with a step size of 0.02 ° (2θ).

Crystalline structures were refined by the Rietveld method [24] with the FullProf software [25]. The peak profiles were modeled by pseudo-Voigt functions. The parameters refined were zero shift (2θ), background, scale factor, unit cell parameters, peak shapes, overall isotropic thermal factors and U, V, W profile parameters (for brookite W was used alone). The quality of the fit was determined visually by inspection of the difference plot and statistically by the goodness of fit (χ^2) defined by:

$$\chi^2 = \Sigma\ w_i(y_{io} - y_{ic})^2/(N - P) \quad (1)$$

where w_i is the weight assigned to each observation, y_{io} and y_{ic} are, respectively the observed and calculated intensities at the ith step, N is the number of points used in the refinement, and P is the number of least-square parameters refined.

The refined FWHM (full-width at half-maximum) of the lines was used to compute, by the Scherrer's equation, the average crystallite size [26]. The instrumental broadening contribution was evaluated by using a highly crystalline rutile sample as the standard.

2.5 Specific surface area, pore size distribution and density

The specific surface areas were computed from the adsorption isotherms, using the Brunauer-Emmett-Teller (BET) method [27]. The adsorbate used was nitrogen and the isotherms were recorded at 77 K, with a Micromeritics ASAP 2,010 M and a Tristar II 3020. The pore size distributions (PSD) were computed from the nitrogen desorption isotherms by the NLDFT method [28] (with Quantachrome Autosorb-1 software using silica equilibrium transition kernel at 77 K, based on a cylindrical pore model).

Skeletal densities of powders were determined using a gas pycnometer (Micromeritics AccuPyc 1330) working with helium. Each experimental value is the average of 10 successive measurements on the same sample.

2.6 Electron microscopy

Conventional TEM observations were performed on a JEOL 1400 operating at 120 kV. Samples were prepared by dipping a carbon-coated grid in a sol diluted 50 times by water. Then the grid was allowed to dry for 48 h at room temperature. Scanning electron microscopy (FEG-SEM) analyses were performed, with a JEOL JSM-6700F, on small glass pieces cut from coated substrates.

3 Results

3.1 Characterization of colloids

3.1.1 XRD

The effect of peptization time on the crystalline structure of the particles is revealed by the XRD patterns of several samples taken from the same sol at different time intervals (Fig. 1). These powder patterns were recorded with xerogels obtained after drying the sol samples at 40 °C. The first one (labelled $t = 0$) was taken at the end of hydrolysis and it was almost completely amorphous. After 1 h, even if the main lines of anatase were identified, the nanoparticles were still predominantly amorphous. After 4 h the particles were nanocrystalline and there was very little difference with a sample taken 6 days after the synthesis. These patterns correspond to a mixture between two titania polymorph, anatase (tetragonal, I41/amd, ICDD PDF#01-073-1764) and brookite (orthorhombic, Pbca, ICDD PDF#00-029-1360).

Comparison between the patterns of samples taken 6 days and 6 months after the synthesis (not shown in Fig. 1) revealed negligible differences. Thus the size and the crystal structure of the nanoparticles are not modified by aging which is proof of the high stability of these sols.

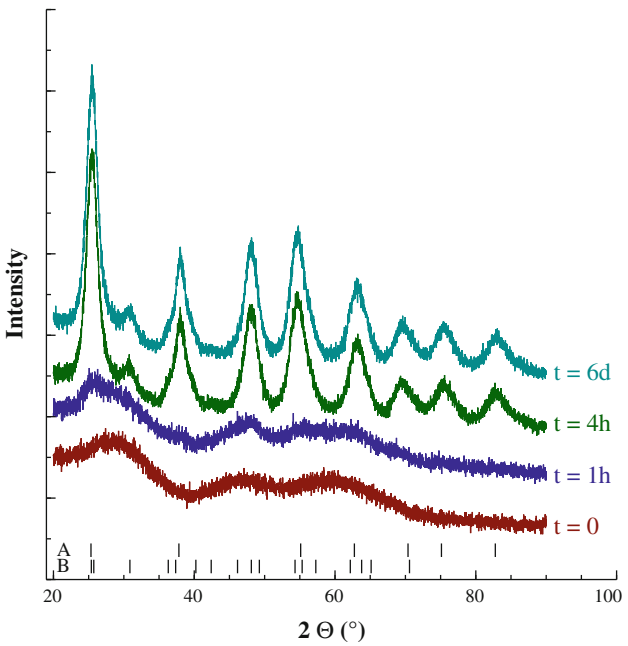

Fig. 1 Effect of peptization time on the XRD patterns of sols dried at 40 °C. Patterns for $t = 4$ h and $t = 6$ days, correspond to a mixture between two titania polymorph, anatase (tetragonal, I41/amd, ICDD PDF#01-073-1764) and brookite (orthorhombic, Pbca, ICDD PDF#00-029-1360)

Rietveld refinements of the diffraction patterns give information on the phase composition, the cell parameters and, from the peak width, the crystallite size of each polymorph. For xerogels prepared in standard conditions and dried below 100 °C, the anatase fraction in the mixture is close to 90%. The anatase cell parameter a is larger (∼3.80 Å) than the value reported for bulk crystals (∼3.78 Å), but the parameter c is lower (9.47 Å instead of 9.49 Å). This has already been observed by Bokhimi et al. [29]. For brookite, a and b parameters are close to the values reported for bulk crystals while c is significantly larger (5.20 Å instead of 5.14 Å). Anatase crystallites have a size close to 5 nm while the size of brookite crystals appears slightly larger (5.6 nm). Upon calcination, the crystallite growth remains small up to 300 °C (∼30%). Above it increases faster; the size at 500 °C is more than two times larger than at 300 °C. Calcination increases also the proportion of brookite (∼17%) and, at 500 °C, 12% of rutile is formed. These data are in agreement with the work of Zhang and Banfield who observed that anatase transforms to brookite and/or rutile, and then brookite further transforms to rutile [30].

When acetylacetone is added (acacH/Ti = 0.5) the peaks of brookite are no more visible on the XRD pattern, the crystallite size decreases to 4 nm, and c parameter becomes close to the value reported for bulk crystals. Conducting hydrolysis with pure water (no peptization) decreases slightly the brookite fraction (∼10%) and increases somewhat the crystallite size (∼20%). Using TIP no diluted in isopropanol has no significant consequence on the crystalline structure and composition.

The polymer (F127 and PEG2000) addition has no significant effect on the cell parameters, however the proportion of rutile and the crystallite size are lower than without polymer. Nevertheless these stabilizing effects decrease when the EO/Ti ratio exceeds 1.5; PEG2000 and F127 give similar stabilizing effects.

3.1.2 TEM

The effect of peptization time on particle morphology was followed using the TEM. Similar to XRD analysis, the TEM was conducted on samples taken from the same sol at different time intervals. The sample taken just at the end of hydrolysis ($t = 0$) was composed of large particles (>300 nm). The top image of Fig. 2 shows a part of one of these particles. They have a "cloudy" aspect which is in agreement with their quasi amorphous structure revealed by XRD. However, at some of their edges facets are visible. After four hours the sol was still essentially composed of large particles (100–200 nm) but now they are clearly observed as nanocrystalline (Fig. 2, center image) with particle size of 4–5 nm. At the end of the peptization, after

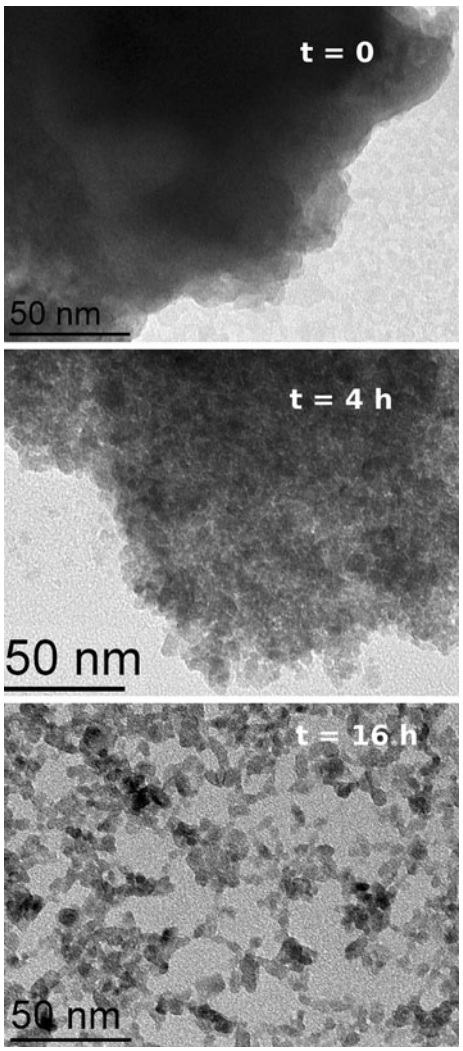

Fig. 2 TEM images of a titania sol for different times after peptization

16 h, the sol contains small chain-like agglomerates having core size of 25–50 nm. These agglomerates are composed of loosely packed crystallites of 5–6 nm. This size is in good agreement with the average size calculated by the Scherrer's equation from the peak width of the XRD patterns.

3.1.3 Zeta potential

The dependence of the ζ-potential on the pH is shown in Fig. 3. When the pH is increased the ζ-potential decreases quickly to the isoelectric point (IEP), which is about 5.4. This value is in good agreement with the data reported in literature [31–37].

When the pH is increased toward the IEP two effects participate resulting in the decrease of the electrophoretic mobility. First the particle surface charge density decreases, second, as no electrolyte was added before the

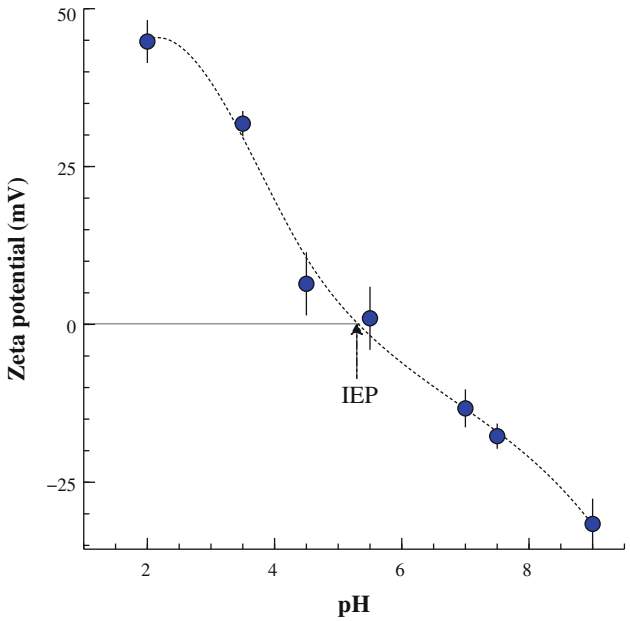

Fig. 3 Dependence of the ζ-potential on the pH. The *dotted lines* are shown for visual aid

electrophoretic mobility titration, the ionic strength increases with pH and there is a compression of the double layer which also reduces the mobility of particles. When increasing the pH further above the IEP, the effects oppose each other as both the ionic strength and the particle surface charge density increase.

3.1.4 Particle size distribution by Dynamic Light Scattering (DLS)

The mean hydrodynamic diameter of particles, measured on freshly prepared sols by dynamic light scattering, was found in the range of 300–500 nm. After a few days of aging the particle diameter decreased to ∼100 nm. This change can be seen by simple observation of the sols appearance. Freshly prepared sols are milky and on aging they become translucent. Our experimental data are in rather good agreement with electron microscopy images and also with the values reported in literature for sols prepared by hydrolysis of titanium alkoxide in large excess of acidified water [22, 31, 38–40]. As reported in literature [31], when the sols are ultrasonicated a marked decrease of particle size, down to 20 nm, is observed.

3.1.5 Rheology

Rheograms were measured by increasing and then decreasing the shear rate. For each rheogram the curves obtained during reversible shear rate-shear stress paths overlapped, *i.e.*, no hysteresis was observed in any of the studied sols. Moreover none of the sols exhibited a Bingham plastic behavior (yield stress can always be approximated to zero). The fitting of the experimental data was done by the power law rheological model [41]:

$$\sigma = K\dot{\gamma}^n \tag{2}$$

where σ is the shear stress (Pa), $\dot{\gamma}$ the shear rate (s^{-1}), K the consistency coefficient, and n the power law index. When the sols show a Newtonian behavior ($n = 1$) K is actually the viscosity, $\eta = \sigma/\dot{\gamma}$.

In the range of 1–1,000 s^{-1} this model has an excellent agreement with the experimental data. Indeed the least square fitting of experimental data with the model always gives correlation coefficients better than 0.9999. The effect of aging, PEG addition and ultrasonication, on K and n parameters, are highlighted in the graphs presented in Fig. 4.

Freshly prepared sols show a shear thinning behavior, with n close to 0.75. On aging this behavior subsides as n tends toward 0.95. Aging has also a strong effect on K, which is reduced to a third of its original value, 6 days after the synthesis. Figure 4a reveals a linear relationship between K and the logarithm of time.

Figure 4c and d shows that the first addition of PEG induces significant (∼50%) decrease of K and a smaller increase (∼10%) of n on a fresh sol. This effect decreases and even vanishes completely upon aging.

Figure 4e shows that ultrasonicating the sol for 30 min strongly decreases K (about 40 times). Irrespective of the age of the sol the value of K after ultrasonication remains the same. Figure 4f shows that, after ultrasonication, n becomes close to 1.

The best fit parameters obtained with a sol prepared without diluting the TIP with isopropanol before hydrolysis are similar to those found for a sol prepared in standard conditions. Thus, although it accelerated the peptization, conducting the hydrolysis with undiluted TIP does not seem to modify the aggregation of the particles in the sol.

Finally the best fit parameters for a sol prepared with addition of acetylacetone to TIP prior to hydrolysis show that this sol has a Newtonian behavior and a low viscosity.

3.2 Characterization of xerogels

3.2.1 Density

The densities of selected powder xerogels, measured with a helium pycnometer, are reported in Table 1. The densities of the xerogels calcined at low temperature (70 °C) are significantly lower ($\rho \sim 3.0$) than the value calculated ($\rho \sim 4$) from the crystal cell parameters for a mixture containing 70% anatase ($\rho = 3.90$) + 30% brookite ($\rho = 4.12$). The density increases with the temperature of

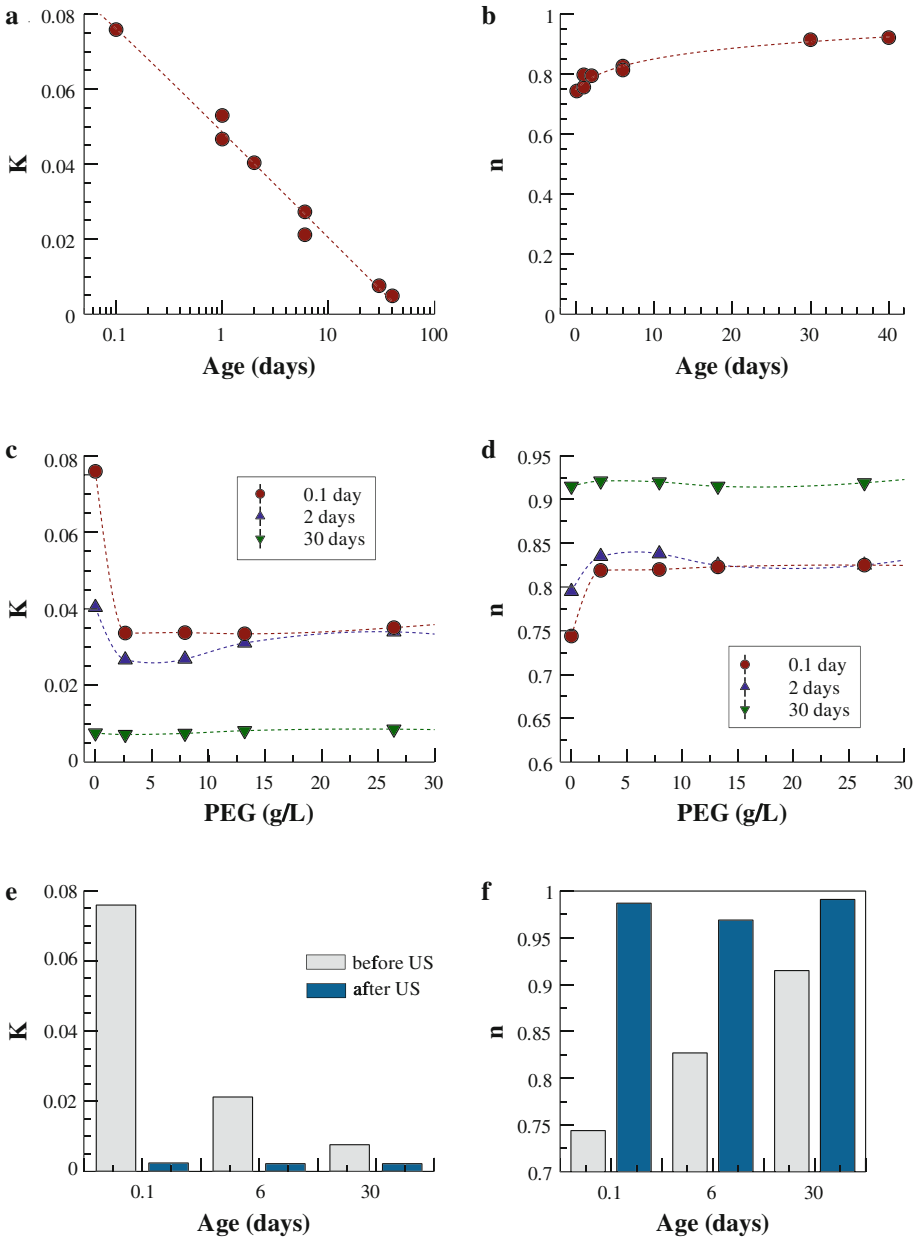

Fig. 4 Best fit parameters *n* and *K* obtained by fitting experimental flow curves by the power law rheological model (Eq. 2). **a** and **b** effect of aging **c** and **d** effect of PEG addition **e** and **f** effect of ultrasonication. Rheometer temperature = 20 °C. The size of the symbols is larger than the standard deviation. The *dotted lines* are shown for visual aid

thermal treatment (Fig. 5a), however, even after calcination at 500 °C, the experimental densities are still lower than the values calculated from cell parameters.

The addition of PEG does not seem to have a significant effect on the density but a good correlation is observed between density and specific surface area (Fig. 5b). Non-peptized sols give xerogels with a higher density than peptized sols (first row of Table 1). The data corresponding to this sample has not been plotted on Fig. 5 graphs.

3.2.2 Specific surface area and porosity

Specific surface area and pore size distribution were computed from the nitrogen adsorption isotherms recorded at 77.4 K. The specific surface areas were calculated using the Brunauer-Emmett-Teller (BET) method [27] and the pore size distributions (PSD) were computed with software based by the NLDFT method [28]. The experimental values obtained with xerogels calcined at various temperatures are reported in Table 2. The isotherms and their corresponding PSD are plotted in Fig. 6.

Xerogels heated at low temperature contains small mesopores and ∼30% of micropores, with pore sizes no larger than 5 nm. Above 300 °C these micropores are eliminated, the pore distribution becomes almost symmetrical, in the range of 3–6 nm. The micropore elimination is accompanied by a small decrease in specific surface area and a significant decrease of the BET C constant. The

Table 1 Effect of calcination temperature and polymer concentration on the density of titania xerogels

Calcination temperature (°C)	PEG (g/L)	BET specific surface area (m^2/g)	Experimental density (g/cm^3)	Relative error (%)	Crystal phases	Crystal density (g/cm^3)
70	0	228	3.278	0.21	A + B	3.90
70	0	196	3.016	0.02	A + B	3.90
200	0		3.190	0.20		
300	0	138	3.510	0.04	A + B	3.94
500	0	63	3.736	0.12	A + B + R	3.97
500	31	124	3.617	0.06	A + B + R	3.94
500	36	131	3.555	0.03	A + B + R	3.94
500	46	117	3.610	0.02	A + B + R	3.95
500	64	101	3.701	0.31	A + B + R	3.95
800	0	1	4.203	0.05	R	4.25

In the last column the crystal density is calculated from cell parameters, taking into account the polymorph composition

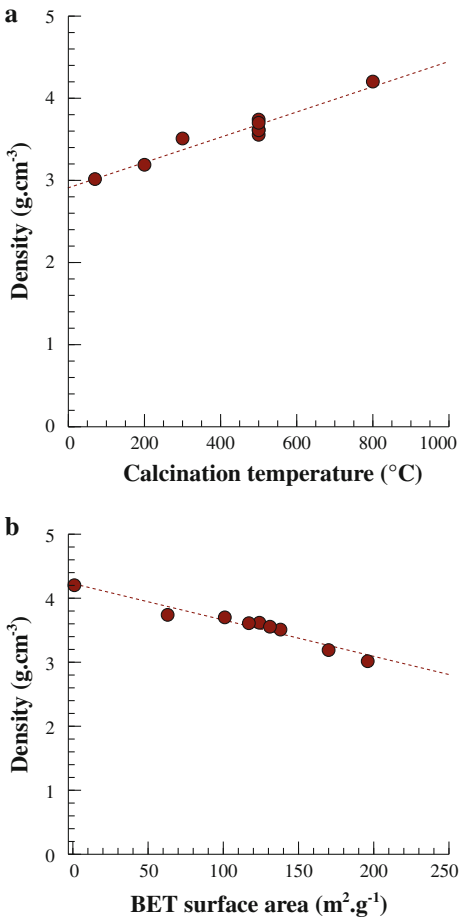

Fig. 5 Correlation between density of titania xerogels and **a** specific surface area (BET). **b** calcination temperature The size of symbols is larger than the standard deviation. The *dotted lines* are shown for visual aid

increase of the average pore size (from 3 to 4 nm) produces an increase in the pore volume. Heating above 300 °C, produces first a shift of the PSD toward larger size (at 400 °C) followed by a decrease in the porosity. Both these effects induce a significant decrease in specific surface area.

The specific surface area S_w (in m^2/g) of a material composed of spherical particles, all having the same diameter D (in nm), can be calculated by the equation:

$$S_w = \frac{6000}{\rho D} \tag{3}$$

where ρ is the density of the crystallites (in g cm^{-3}). Using the cell parameters, the crystallite size and the polymorph composition obtained from the analysis of XRD patterns, it is possible to calculate the specific surface area. When these calculated values, spanning a range from 0 to about 200 m^2/g, were plotted against the BET surface area for a set of 25 xerogels surprisingly, despite the large approximation implied in this kind of calculation, a linear correlation was observed (coefficient correlation = 0.988). The slope of the regression line is about 0.76 which could mean that only 76% of the crystallite surface is accessible to adsorbent molecules.

In parallel to the XRD study reported above, the effect of peptization time on the surface and porosity of the xerogel had been examined. However, it should be mentioned that the samples were all degassed at 300 °C before the adsorption analysis. The main results are summarized in Table 3. The isotherms and their corresponding PSD are shown in Fig. 7. The first sample, taken at the end of hydrolysis, contains only a few small mesopores, in the range of 2–6 nm. The main nitrogen uptake (66%) is observed above a relative pressure of 0.9, which corresponds to slit pores with pore size larger than 20 nm. This porosity probably results from the stacking of the large particles observed on TEM images (Fig. 2).

After 60 min of peptization, small mesopores are formed, giving a sharp peak centered at 3 nm. At this point a significant adsorption (30%) above the relative pressure

Table 2 Effect of the calcination temperature on the textural characteristics of xerogel samples prepared in standard conditions

Calcination temperature (°C)	BET			Isotherm		Porosity	NLDFT		
	Surface area (m^2/g)	C	CC	Pore vol (cm^3/g)	D_h (nm)		Fit error (%)	S_{cum} (m^2/g)	V_{cum} (cm^3/g)
50	236	181	0.99987	0.12	2.0	0.27	0.23	236	0.11
100	237	150	0.99996	0.12	2.0		0.57	249	0.11
200	223	60	0.99997	0.13	2.3	0.29	0.57	203	0.12
300	221	33	0.99996	0.14	2.5	0.33	0.40	169	0.14
400	124	55	0.99994	0.13	4.2	0.32	0.47	98	0.13
500	62	61	0.99998	0.08	5.2	0.24	0.71	58	0.08

When the density of the sample has been measured, we have calculated the porosity. CC is the correlation coefficient of the least-squares fit performed on the BET plot and C is the BET constant. The hydrodynamic diameter D_h is calculated from surface area and pore volume assuming that pores are cylindrical, $D_h = 4$ V/S

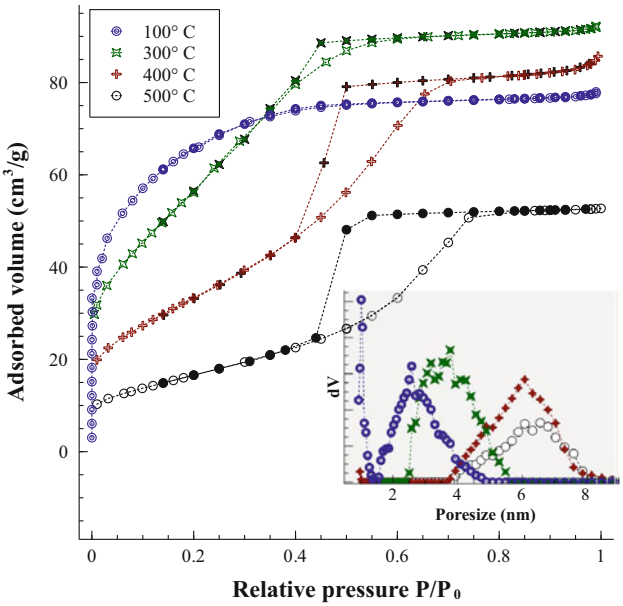

Fig. 6 Effect of calcination temperature on N_2-adsorption isotherms (*bold symbols* correspond to the desorption branch) and PSD (*inset graph*) computed from N_2-adsorption isotherms by the NLDFT method [28] (with Quantachrome Autosorb-1 software using silica equilibrium transition kernel at 77 K, based on a cylindrical pore model)

of 0.9 is still observed. After 240 min there is a strong increase in the volume of mesopores associated with a shift toward larger size. The adsorption above the relative pressure of 0.9 is still present but it represents only 6% of the total pore volume.

3.2.3 *Thermal analysis*

Figure 8 shows the thermogram recorded for a xerogel dried at 40 °C prepared without acid addition. The total mass loss is about 8%. Mass spectrometry analysis of the evolved gas reveals only traces of carbon species (CO_2), thus, the mass loss is essentially a loss of water. DTG curve shows that the dehydration process occurs in two steps at least. However, a far better fit of the DTG curve is obtained if a third peak is added. Based on the shape of the first peak, Gaussian-type peak was used for the fitting; the peak parameters are reported in Table 4. As all the peaks start at the beginning they most likely correspond to parallel processes. The first peak has a maximum at 106 °C and ends just after 200 °C. In this experiment it corresponds to a mass loss of less than 3%, however, the area of this peak is closely related to the drying time and temperature. This low temperature dehydration is usually attributed to the removal of weakly adsorbed water.

Table 3 Effect of the peptization time on the textural characteristics of xerogels samples

Peptization time (min)	BET			Isotherm		NLDFT		
	Surface area (m^2/g)	C	CC	Pore vol cm^3/g	D_h (nm)	Fit error (%)	S_{cum} (m^2/g)	V_{cum} (cm^3/g)
0	34	179	0.99971	0.08	9.4	0.44	30	0.05
60	122	167	0.99956	0.09	3.0	0.13	109	0.08
240	238	51	0.99993	0.15	2.5	0.33	202	0.14

CC is the correlation coefficient of the least-squares fit performed on the BET plot and C is the BET constant. The hydrodynamic diameter D_h is calculated from surface area and pore volume assuming that pores are cylindrical, $D_h = 4$ V/S

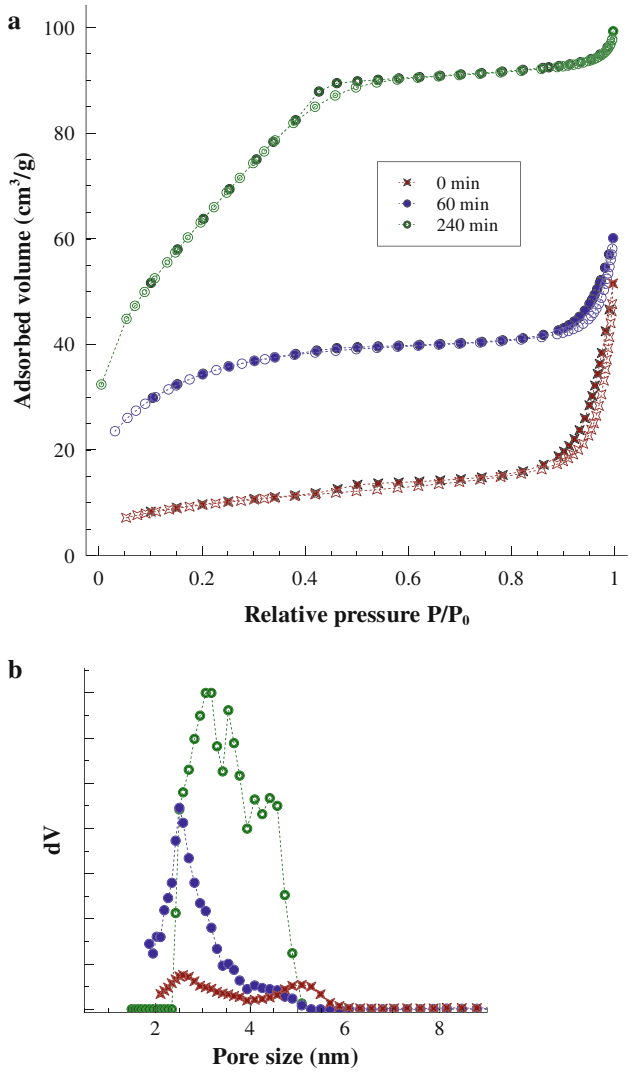

Fig. 7 Effect of peptization time on: **a** N_2-adsorption isotherms (bold symbols correspond to the desorption branch). **b** PSD computed from N2-adsorption isotherms by the NLDFT method [28] (with Quantachrome Autosorb-1 software using silica equilibrium transition kernel at 77 K, based on a cylindrical pore model)

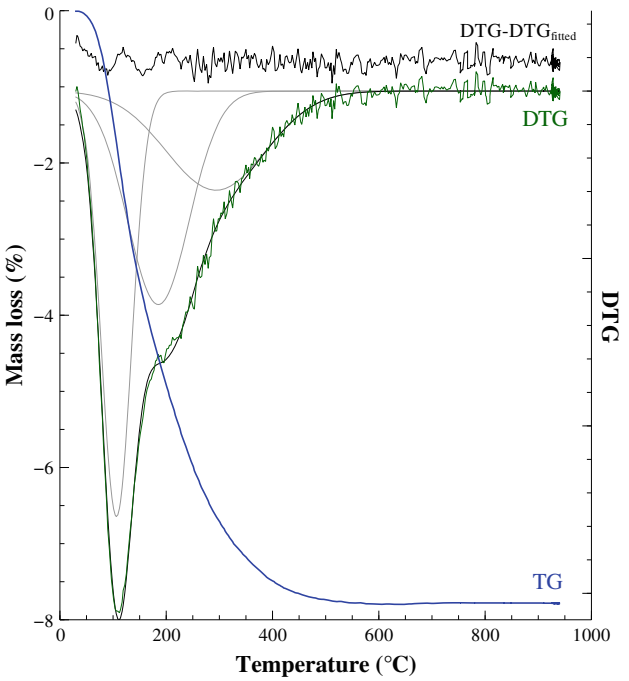

Fig. 8 Thermogravimetric analysis of a xerogel dried at 40 °C and prepared without acid addition. This plot shows the experimental TG and DTG curves as well as the best fit of the DTG curve by three parallel dehydration processes. The top curve corresponds to the difference between the experimental curve and the sum of peaks. Gaussian-type peak was used for the fitting

Table 4 Peak parameters for the decomposition of DTG curve of non peptized sample of Fig. 8

Peak no.	T_{max} (°C)	FWHM (°C)	Area (in wt% water)
1	106	67	2.8
2	185	137	2.9
3	294	220	2.1

Gaussian-type peak was used for the fitting

The second process, representing a mass loss of 2.9%, gives a broader peak with a maximum at 185 °C which ends at ~350 °C. The water released in this step corresponds to the dehydroxylation of the particle surface. A quick decrease in surface area and porosity is observed from a temperature close to the elimination of these hydroxyl species (Table 2). From the amount of water lost in this step, the number of hydroxyl group per Ti atom was calculated; we found OH/Ti ~0.28. Now from this value and the specific surface area, an approximate surface OH density can be calculated. Using a surface area of 330 m^2/g (value calculated with Eq. 3) for particles having a density of 3 g/cm^3 and a diameter of 6 nm) we found 6.3 OH/nm^2. This value is in good agreement with those already reported for large surface area titania (~6 OH/nm^2) [42].

The third process gives a very broad peak (FWHM ~ 220 °C). Its maximum is close to 300 °C and it ends at 550 °C. We attribute this peak to the slow removal of the hydroxyl groups trapped inside the particles. This is a limited diffusion process which ends with anhydrous titania. As already reported in a previous study [43] the removal of these remaining defects corresponds precisely to the temperature where the exothermal crystallization into rutile of the metastable anatase and brookite phases is observed.

The presence of OH groups inside the crystalline structure has already be related to the titanium deficiency given by the Rietveld refinement [29]. It could also explain why the density of xerogels calcined at 500 °C is lower than that calculated from the cell parameters (Table 1). Thermal analysis of a peptized sol has been reported before

[43] and, in this case, the mass loss is the sum of nitrate decomposition and water loss.

4 Discussion

4.1 Synthesis of stable sols

Hydrolysis of titanium alkoxide in a large excess of water, followed by peptization, is a fast and easy method to prepare colloidal dispersions of titania nanocrystallites in water [21, 23, 31, 39, 40, 44–47]. The main parameters which have been recognized as effective to control the size and the stability of the colloids are the water/alkoxide and acid/alkoxide ratios, the temperature, and the alcohol concentration.

The first step is to obtain particles of the smallest possible dimension by maximizing the hydrolysis rate with respect to condensation. This is achieved by using a large excess of acidified water because titanium isopropoxide is monomeric and very reactive; it can be rapidly and completely hydrolyzed under acid conditions before condensation starts [48]. The optimum ratio of water to alkoxide appears to be in the range of 50–100 because it was shown that above 200 the effect of dilution on particle size becomes negligible [47] and, using ratio larger than 100, leads to stable but too diluted sols which will require preliminary concentration before being used for coatings. On the other hand, for values lower than 30, some OR groups can persist due to incomplete hydrolysis [11, 49].

The nanoparticles formed by this rapid hydrolysis have a high surface energy and they agglomerate rapidly, producing large particles which precipitate. As shown in Figs. 1 and 2 these particles are amorphous because, due to the fast nucleation rate, the particle growth is governed by kinetics leading to the formation of the less stable phase [50]. But this phase is also the most soluble and it will be progressively replaced by the crystalline phases like brookite, anatase and rutile. The rate of this crystallization process depends on the pH and temperature which govern the solubility.

The second step is the peptization, which starts immediately if acidified water is used, or after the post addition of acid. As the PZC is close to neutrality, acid addition results in protonation of surface hydroxyls, increasing the electrostatic surface charge density of the particles, and decreasing the interfacial tension [51–53]. This causes the fragmentation of primary particle agglomerates and also, as the colloidal particles bear a same sign electric charge, this prevents their re-aggregation because they mutually repel each other.

In contrast to hydrolysis, peptization is a slow process that exhibits first-order kinetics [39] with time constants of several days [22]. Kinetics studies have shown that the peptization is slow because it is the result of the simultaneous action of two opposing mechanisms, the fragmentation of agglomerates, which is mediated by the peptizing agent, and the reagglomeration of the fragments, which is driven by insufficient stabilization of the suspension [22, 40, 44]. Peptization time can be reduced by increasing either the temperature or the acid concentration [50]. However, this has negative side effects. Decreasing the pH and increasing temperature increases the titania solubility, leading to the growth of larger particles at the expense of smaller ones by a classical dissolution-reprecipitation mechanism (Ostwald ripening). Moreover secondary particles are formed by epitaxial self-assembly of primary particles [21]. Another side effect of increasing the titania solubility is the progressive transformation of metastable crystalline phases, like brookite and anatase, into rutile which is the stable phase. Thus to prepare highly stable sols it is mandatory to use an acid concentration close to the minimum amount required for peptization. If needed, the peptization time can be reduced by ultrasonication.

At this point a question arises, what is the best peptizing agent, HCl or HNO_3? Isley and Penn have shown that using HCl increases the amorphous content [23]. On aging this amorphous phase will recrystallize into stable rutile. This was used as a method to prepare nanocrystallites of rutile [54]. On the other hand HNO_3 is easily decomposed by heating above 300 °C while it is far more difficult to remove chloride ions without extensive washings. Thus, except if the rutile phase is desired, HNO_3 seems a better choice.

Another important parameter, often neglected, is the presence of alcohol. Vorkapic and Matsoukas have shown that alcohols have a negative effect on the peptization [40]. They explain this effect by the decrease of the dielectric constant of the solvent leading to an enhanced rate of reaggregation. It is also possible that alcohol stabilizes the amorphous phase formed just after the hydrolysis. Consequently removal of the alcohol reduces the peptization time and stabilizes the sol. The presence of alcohol cannot be avoided since, even if no alcohol is added to dilute the alkoxide, four moles of isopropanol per mole of TIP are formed as a product of hydrolysis. Probably the easiest way of removing isopropanol is by evaporation, by conducting the peptization in an open flask at a temperature close to the boiling point of the azeotrope isopropanol-water (80.3 °C).

It is very common to dilute the alkoxide in isopropanol prior to mixing with water in order to reduce the relatively high viscosity of the TIP. This is supposed to provide a more homogeneous nucleation and reduce the growth process. However, we observed negligible differences in crystallite size when isopropanol was not added.

In summary, in order to produce highly stable hydrosols composed of crystallites of the smallest dimension possible, the optimized synthesis conditions come out to be: using $[H_2O]/[Ti]$ in the range of 50–100, HNO_3 as catalyst and peptizing agent with $[H^+]/[Ti] = 0.2$, hydrolysis temperature in the range of 50–70 °C, peptization temperature close to 80 °C and allowing isopropanol to evaporate. These sols will be made up of small aggregates ($\sim$100 nm) of anatase ($\sim$90%) and brookite crystallites (5–6 nm).

It is also possible to prepare stable sols, composed solely of anatase crystallites (4 nm), by complexing partially the TIP by acetylacetone before hydrolysis. Acetylacetone (AcacH) reacts with titanium alkoxides to form mixed complexes which are more difficult to hydrolyze than alkoxy group [48]. Upon hydrolysis alkoxy groups quickly react while all Acac ligands cannot be cleaved even in presence of a large excess of water [55]. This inhibits the condensation and either molecular clusters or colloidal particle can be synthesized depending of the relative importance of complexing (AcacH/Ti) versus hydrolysis (H_2O/Ti) [56]. Slowing down the condensation favors anatase formation (slightly more stable than brookite) and gives smaller crystallites.

The knowledge of the rheological behavior of sols is mandatory to control the thickness of the coatings. Moreover it gives important information on the interaction between the particles as well as on aggregate morphology. We have seen that the flow curves of these titania colloids can be accurately fitted, in the range of 0–1,000 s^{-1}, with a power law model. In a previous study [57] we have observed that the viscosity dependence on particle concentration can be predicted by a Batchelor-type model [58] provided the volume fraction of particles was replaced by an effective volume fraction of aggregates taking into account their fractal dimension.

The shear thinning behavior, observed with freshly prepared sols, is explained because primary particles have a strong tendency to form aggregates with a chainlike structure (Fig. 2). The packing density of these clusters decreases from the center to the edges and it seems probable that the outer edge particles could be disconnected from such aggregates at high shear rates.

The decrease of viscosity on aging is explained by a progressive reorganization of the aggregates towards a more compact packing because the slow peptization will gradually increase the surface charge of the particles decreasing the sticking probability.

We observed that the first addition of PEG induced a marked decrease of the sol viscosity (Fig. 4). This effect has been already reported both for PEG 2000 [57] and Pluronic F127 [43]. It was explained by assuming that polymer adsorption on the titania particles induces a stabilization by steric effect which in turn decreases the sticking probability, and leads to progressive reorganization of the aggregates toward a more compact packing. This also explains why this effect decreases and even vanishes totally upon aging.

It should be emphasized that long term aging affects the particle organization but does not change either the primary particle size or the polymorph composition. This is confirmed by the perfect overlapping of the XRD pattern recorded on a fresh sol with the pattern recorded 6 months latter.

Addition of acetylacetone to TIP prior to hydrolysis gives a sol composed only of anatase crystallites having a viscosity similar to an aged sol showing a Newtonian behavior. This is consistent with small and compact aggregates and can be explained by adsorption, on the surface of anatase crystals, of acetylacetone released during the hydrolysis of the complex.

Ultrasonication is a very efficient way to break the aggregates (Fig. 4f). The final aggregate size is the same, irrespective of the age of sol, and the low viscosity observed is in agreement with the particle size given by DLS, $\sim$20 nm, which corresponds to aggregates containing just a few primary particles. This was already reported by Xu et al. [59].

4.1.1 Microstructure of xerogels

We have observed that experimental density is lower than the crystal density (Table 1). One cause could be the presence of closed porosity. However, the good correlation observed between experimental density and the BET specific surface area (Fig. 5b) let us suppose that experimental density is lower because there is a layer, at the surface of the particles, containing adsorbed water and hydroxyl groups. The global density ρ of this material will be:

$$\rho = \frac{m_{\text{layer}} + m_{\text{crystal}}}{V_{\text{layer}} + V_{\text{crystal}}}$$

For 1 g of material, $m_{\text{layer}} + m_{\text{crystal}} = 1$ and $V_{\text{crystal}} = \frac{m_{\text{crystal}}}{\rho_{\text{crystal}}} = \frac{1 - m_{\text{layer}}}{\rho_{\text{crystal}}}$ which leads to: $\rho = \frac{1}{V_{\text{layer}} + \frac{1 - m_{\text{layer}}}{\rho_{\text{cryst}}}}$.

We can consider that m_{layer} is the mass loss given by the thermal analysis (actually a part has been attributed to the removal of hydroxyl groups inside the particles but this also contributes to the lowering of density). For a non peptized sample, it corresponds to water, and $V_{\text{layer}} = m_{\text{layer}} \sim 0.08$ g (8%) which leads to $\rho \sim 3.23$. This is close to the experimental density $\rho_{\text{exp}} = 3.28$ (first row of Table 1).

For peptized sample, the mass loss given by the thermal analysis is the sum of water and nitrate decomposition, and $m_{\text{layer}} \sim 0.23$ g (23%). However we do not know the

density of this layer containing water and nitrate. Assuming that $V_{layer} = m_{layer}$ leads to $\rho \sim 2.37$ which is obviously too low compared to the measured density (~ 3.0).

From the pore volume of the xerogels, V_{pore} and their density, ρ it is possible to calculate their porosity by the relation:

$$\varepsilon = \frac{\text{volume of pores}}{\text{total volume}} = \frac{V_{pore}}{V_{pore} + \frac{1}{\rho}} \quad (4)$$

The xerogels resulting from the drying of the peptized sols at low temperature (<100 °C) have a pore volume of 0.12 cm^3/g (Table 2) and a density of 3 (Table 1). This gives a porosity of 0.27. This value is very close to the porosity of a material resulting from close packing of spherical particles (0.26). Moreover the pore size distribution is also in very good agreement with a similar material having a spherical shape with a diameter of 6 nm, since we observed two peaks at about 1 and 2.5 nm (Fig. 6), corresponding, respectively to the tetrahedral ($6 \times 0.225 \sim 1.4$) and octahedral ($6 \times 0.414 \sim 2.5$) holes.

Thus, as already reported by Xu and Anderson [31, 59], during the drying the particles arrange to form a compact material. Due to electrostatic repulsion, which reduces sticking probability, particle aggregation follows a reaction-limited model and produces dense aggregates.

When the xerogels are heated in air there is an increase of the porosity up to 300 °C ($\varepsilon = 0.33$) because the loss of weakly bond water and the dehydroxylation are not compensated by the reorganization of the particles. However, the gain in porosity remains limited. Above 300 °C the surface hydroxyls, which prevented direct contact between crystallites, are almost eliminated (Fig. 8). A progressive growth of the crystallites will occur inducing a reorganization of the particles accompanied by shrinkage of the porosity.

Finally it would be quite difficult to obtain, without additives, porous films from aqueous sols stabilized by electrostatic repulsion since they always give compact materials on drying. Xu and Anderson [31] have shown that, in reducing the repulsive energy by increasing the pH, the mechanism of aggregation follows a diffusion-limited model, resulting in spongy structures with porosity which can exceed 0.5. This of course, leads to unstable sols due to the reduction in repulsive energy.

To prepare coatings with controlled porosity from stable hydrosols, a strategy consists of adding a polymer which adsorbs at the surface of the particles. During the drying step the polymer will coat the particles and, with a suitable calcination process, the porosity left by polymer removal can be retained. As the coordination number is decreased thermal stabilization is improved [60]. For example addition of polyethylene glycol (PEG) in titania hydrosols can significantly improve the surface area and the porosity of the xerogels obtained after calcination [54, 61]. Addition of PEG induces an increase of the number of pores, a shift towards larger pore size, and a broadening of the pore size distributions. But there is an optimum value for the amount of PEG, above which the porosity and the surface area decrease [10].

Furthermore another advantage of addition of PEG is the elimination of the film cracking and peeling off the substrate very often observed, especially on steel substrates, as soon as the film exceed a critical thickness [19, 61].

If the polymer is a non-ionic surfactant, like block copolymers of poly(oxyethylene)-poly(oxypropy1ene)-poly(oxyethylene)polyethylene, self-assembly (spontaneous formation of complex hierarchical structures from predesigned building blocks [62]) can occur. This allows an even better control of the porosity. For example addition of Pluronic F127 provides a higher surface area and porosity than an equivalent amount of PEG2000 [10]. The

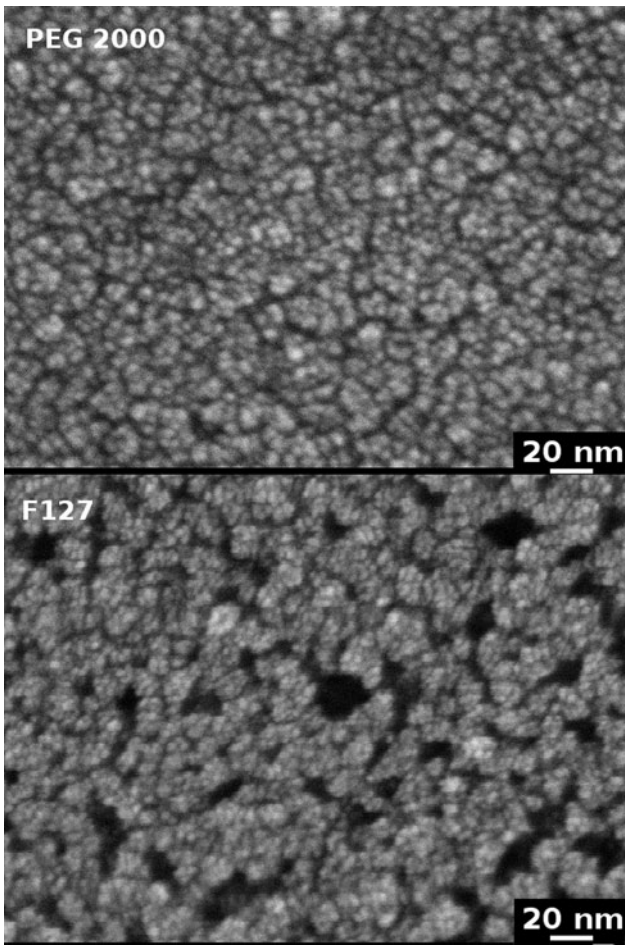

Fig. 9 SEM images of the top surface of a glass plate coated with a TiO_2 sol containing PEG 2000 (*top*) and Pluronic F127 (*bottom*). In both cases the amount of polymer corresponds to EO/Ti = 1

SEM images presented in Fig. 9 show the strong textural differences between coatings done with sols containing either PEG2000 or F127. With the copolymer, the large porosity resulting from the formation of micelles is clearly visible.

Temperature required for total oxidation of the polymer can be lowered by taking advantage of the photocatalytic activity of the titania films; a UV irradiation is applied before the calcination [63, 64].

Another advantage of polymer addition is obtained if the polymer is strongly anchored on the surface of particles because the sol stability is improved through steric stabilization [62, 65]. For example the adsorption of PEG on the surface of titania nanoparticles is due to the formation of hydrogen bonds between the titania hydroxyl groups and either the terminal hydroxyls of PEG (tail adsorption) or one of the oxygen lone pairs of electrons in PEG ethoxy groups (train and loop adsorption).

5 Summary

To synthesize, by hydrolysis of the titanium isopropoxide, nanocrystallite dispersions of titania in water, suitable for coatings and having long-term stability (more than 1 year) in terms of polymorphic composition, crystallite and agglomerate size, we found that the best experimental conditions are:

(i) water/alkoxide ratio in the range of 50–100
(ii) H^+/alkoxide ratio close to 0.2, HNO_3 being preferred vs HCl
(iii) peptization temperature allowing the fast removal of isopropanol by evaporation (about 80 °C).

In these conditions the sols are composed of aggregates, with a chainlike structure, of anatase ($\sim$90%) and brookite crystallites (5–6 nm). On aging a progressive reorganization of the aggregates toward a more compact packing occurs. This rearrangement is accompanied by a marked decrease of the viscosity. It can be quickly obtained by ultrasonication.

Stable sols composed solely of anatase crystallites (4 nm) can be prepared by complexing partially the TIP by acetylacetone before hydrolysis.

It is not possible to produce porous films from these sols stabilized by electrostatic repulsion because, during the drying step, the particles arrange to form materials with a close packed structure. However, coatings with controlled porosity can be prepared from these hydrosols through the addition of polymers, like PEG or block copolymers.

Acknowledgment The authors thank Dr. Djar Oquab (CIRIMAT) for the FEG-SEM images.

References

1. O'Regan B, Gratzel BM (1991) A low-cost, high-efficiency solar cell based on dye-sensitized colloidal TiO_2 films. Nature 353:737–740
2. Fox MA, Dulay MT (1993) Heterogeneous photocatalysis. Chem Rev 93:341–357
3. Linsebigler AL, Lu G, Yates JT (1995) Photocatalysis on TiO_2 surfaces: principles, mechanisms, and selected results. Chem Rev 95:735–758
4. Bhatkhande DS, Pangarkar VG, Beenackers A (2002) Photocatalytic degradation for environmental applications—a review. J Chem Technol Biotechnol 77:102–116
5. Carp O, Huisman CL, Reller A (2004) Photoinduced reactivity of titanium dioxide. Prog Solid State Chem 32:33–177
6. Hashimoto K, Irie H, Fujishima A (2005) TiO_2 photocatalysis: a historical overview and future prospects. Jpn J Appl Phys 44: 8269–8285
7. Tauster SJ, Fung SC, Garten RL (1978) Strong metal-support interactions. Group 8 noble metals supported on TiO_2. J Am Chem Soc 100:170–175
8. Haruta M (1997) Size- and support-dependency in the catalysis of gold. Catal Today 36:153–166
9. Haruta M (2002) Catalysis of gold nanoparticles deposited on metal oxides. Cattech 6:102–115
10. Alphonse P, Ansart F (2009) Catalytic coatings on steel for low temperature propane pre- reforming to SOFC application. J Colloid Interface Sci 336:658–666
11. Yoldas BE (1986) Hydrolysis of titanium alkoxide and effects of hydrolytic polycondensation parameters. J Mater Sci 21: 1087–1092
12. Yu J, Zhao X, Zhao Q (2000) Effect of surface structure on photocatalytic activity of TiO_2 thin films prepared by sol-gel method. Thin Solid Films 379:7–14
13. Yu J, Zhao X, Du J, Chen W (2000) Preparation, microstructure and photocatalytic activity of the porous TiO_2 Anatase coating by Sol–Gel processing. J Sol–Gel Sci Technol 17:163–171
14. Kim DJ, Hahn SH, Oh SH, Kim EJ (2002) Influence of calcination temperature on structural and optical properties of TiO_2 thin films prepared by sol–gel dip coating. Mater Lett 57: 355–360
15. Legrand-Buscema C, Malibert C, Bach S (2002) Elaboration and characterization of thin films of TiO_2 prepared by sol-gel process. Thin Solid Films 418:79–84
16. Zhang L, Zhu Y, He Y, Li W, Sun H (2003) Preparation and performances of mesoporous TiO_2 film photocatalyst supported on stainless steel. Appl Catal B 40:287–292
17. Bu S, Jin Z, Liu X, Yang L, Cheng Z (2004) Fabrication of TiO_2 porous thin films using PEG templates and chemistry of the process. Mater Chem Phys 88:273–279
18. Bu SJ, Jin ZG, Liu XX, Yang LR, Cheng ZJ (2005) Synthesis of TiO_2 porous thin films by polyethylene glycol templating and chemistry of the process. J Eur Ceramic Soc 25:673–679
19. Guo B, Liu Z, Hong L, Jiang H (2005) Sol gel derived photocatalytic porous TiO_2 thin films. Surf Coat Technol 198:24–29
20. Djaoued Y, Thibodeau M, Robichaud J, Balaji S, Priya S, Tchoukanova N, Bates SS (2008) Photocatalytic degradation of domoic acid using nanocrystalline TiO_2 thin films. J Photochem Photobiol A Chem 193:271–283
21. Oskam G, Nellore A, Penn RL, Searson PC (2003) The Growth Kinetics of TiO_2 Nanoparticles from Titanium(IV) Alkoxide at High Water/Titanium Ratio. J Phys Chem B 107:1734–1738
22. Vorkapic D, Matsoukas T (1999) Reversible Agglomeration: A Kinetic Model for the Peptization of Titania Nanocolloids. J Colloid Interface Sci 214:283–291

23. Isley SL, Lee Penn R (2006) Relative Brookite and Anatase Content in Sol-Gel-Synthesized Titanium Dioxide Nanoparticles. J Phys Chem B 110:15134–15139
24. Rietveld HM (1969) A profile refinement method for nuclear and magnetic structures. J Appl Crystallogr 2:65–71
25. Rodríguez-Carvajal J (2001) Recent developments of the program FULLPROF. Commission on powder diffraction (IUCr). News Lett 26:12–19
26. Patterson AL (1939) The Scherers Formula for X-Ray particle size determination. Phys Rev 56:978–982
27. Brunauer S, Hemmett P, Teller E (1938) Adsorption of gases in multimolecular layers. J Am Chem Soc 60:309–319
28. Seaton N, Walton J, Quirke N (1989) A new analysis method for the determination of the pore size distribution of porous carbons from nitrogen adsorption measurements. Carbon 27:853–861
29. Bokhimi X, Morales A, Novaro O, Lopez T, Sanchez E, Gomez R (1995) Effect of hydrolysis catalyst on the Ti deficiency and crystallite size of sol–gel–TiO_2 crystalline phases. J Mater Res 10:2788–2796
30. Zhang H, Banfield JF (2000) Understanding polymorphic phase transformation behavior during growth of noncrystalline aggregates: insights from TiO_2. J Phys Chem B 104:3481–3487
31. Xu Q, Anderson MA (1991) Synthesis of porosity controlled ceramic membranes. J Mater Res 6:1073–1081
32. Kosmulski M, Matijevic E (1992) Zeta potential of anatase (TiO_2) in mixed solvents. Colloids Surf 64:57–65
33. Yang Hua-Gui, Li Chun-Zhong, Gu Hong-Chen, Fang Tu-Nan (2001) Rheological behavior of titanium dioxide suspensions. J Colloid Interf Sci 236:96–103
34. Kosmulski M (2002) The significance of the difference in the point of zero charge between rutile and anatase. Adv Colloid Interface Sci 99:255–264
35. Preocanin T, Kallay N (2006) Point of zero charge and surface charge density of TiO_2 in aqueous electrolyte solution as obtained by potentiometric mass titration. Croatica Chemica Acta 79:95–106
36. Ridley MK, Hackley VA, Machesky ML (2006) Characterization and Surface-Reactivity of noncrystalline anatase in aqueous solutions. Langmuir 22:10972–10982
37. Fazio S, Guzman J, Colomer MT, Salomoni A, Moreno R (2008) Colloidal stability of nanosized Titania aqueous suspensions. J Eur Ceramic Soc 28:2171–2176
38. Anderson MA, Gieselmann MJ, Xu Q (1988) Titania and alumina ceramic membranes. J Membr Sci 39:243–258
39. Bartlett JR, Woolfrey JL (1992) Peptization of hydrous Titania. In: Hench LL, West JK (eds) Chemical processing of advanced materials. Wiley, New York, pp 247–256 Chapter 23
40. Vorkapic D, Matsoukas T (1998) Effect of temperature and alcohols in the preparation of Titania nanoparticles from alkoxides. J Am Ceram Soc 81:2815–2820
41. Goodwin JW, Hughes RW (2002) Rheology for chemists: an introduction. The Royal Society of Chemistry, London, p 6
42. Mueller R, Kammler HK, Wegner K, Pratsinis SE (2003) OH surface density of SiO_2 and TiO_2 by thermo gravimetric analysis. Langmuir 19:160–165
43. Bleta R, Alphonse P, Lorenzato L (2010) Nanoparticles route for the preparation in aqueous medium of mesoporous TiO_2 with controlled porosity and crystalline framework. J Phys Chem C 114:2039–2048
44. Bartlett JR, Woolfrey JL (1992) Production of sols from aggregated Titania precipitates, In: Better ceramics through chemistry V: materials research society symposium proceedings. Materials Research Society, Pittsburg (Pa), 271:309–315
45. So WW, Park SB, Kim KJ, Shin CH, Moon SJ (2001) The crystalline phase stability of Titania particles prepared at room temperature by the sol–gel method. J Mater Sci 36:4299–4305
46. Bosc F, Ayral A, Albouy PA, Guizard C (2003) A simple route for low-temperature synthesis of mesoporous and nanocrystalline anatase thin films. Chemistry of Materials 15:2463–2468
47. Cordero-Cabrera M, Walker G, Grant D (2005) Effect of processing parameters on the particle size and stabilisation of Titania sols. J Mater Sci 40:3709–3714
48. Sanchez C, Livage J (1990) Sol–gel chemistry from metal alkoxide precursors. New J Chem 14:513–521
49. Terabe K, Kato K, Miyazaki H, Yamaguchi S, Imai A, Iguchi Y (1994) Microstructure and crystallization behaviour of TiO_2 precursor prepared by the sol–gel method using metal alkoxide. J Mater Sci 29:1617–1622
50. Bischoff BL, Anderson MA (1995) Peptization process in the Sol–Gel preparation of porous anatase (TiO_2). Chem Mater 7:1772–1778
51. Bancroft WD (1916) The theory of peptization. J Phys Chem 20:85–117
52. Sen KC (1925) On the theory of peptization. J Phys Chem 29:1533–1547
53. Pottier A, Cassaignon S, Chaneac C, Villain F, Tronc E, Jolivet JP (2003) Size tailoring of TiO_2 anatase nanoparticles in aqueous medium and synthesis of nanocomposites. Characterization by Raman spectroscopy. J Mater Chem 13:877–882
54. Bosc F, Ayral A, Keller N, Keller V (2007) Room temperature visible light oxidation of CO by high surface area rutile TiO_2-supported metal. Applied Catalysis B 69:133–137
55. Bleuzen A, Barboux-Doeuff S, Flaud P, Sanchez C (1994) Rheological study of titanium oxide-based gels. Mater Res Bull 29:1223–1232
56. Julbe A, Guizard C, Larbot A, Mouchet C, Vacassy R, Metz R, Cot L (1994) Sol–gel processing of zirconia and titania membrane. In: Proceeding of the international conference on inorganic membranes, Worcester MA USA, pp 17–25
57. Alphonse P, Bleta R, Soules R (2009) Effect of PEG on rheology and stability of nanocrystalline Titania hydrosols. J Colloid Interf Sci 337:81–87
58. Batchelor GK (1977) The effect of Brownian motion on the bulk stress in a suspension of spherical particles. J Fluid Mech 83:97–117
59. Xu Q, Gieselmann MJ, Anderson MA (1989) The colloid chemistry of ceramic membranes. Poly Mater Sci Eng 61: 889–893
60. Kumar KNP, Engell J, Kumar J, Keizer K, Okubo T, Sadakata M (1995) Pore-structure stabilization by controlling particle coordination. J Mater Sci Lett 14:1784–1788
61. Miki T, Nishizawa K, Suzuki K, Kato K (2004) Preparation of thick TiO_2 film with large surface area using aqueous sol with poly (ethylene glycol). J Mater Sci 39:699–701
62. Dutta J, Hofmann H (2003) Self-organization of colloidal nanoparticles. In: Nalwa HS (ed) Encyclopedia of nanoscience and nanotechnology, vol X. pp 1–23. www.aspbs.com/enn
63. Bosc F, Ayral A, Albouy PA, Datas L, Guizard C (2004) Mesostructure of anatase thin films prepared by mesophase templating. Chem Mater 16:2208–2214
64. Bosc F, Lacroix-Desmazes P, Ayral A (2006) TiO_2 anatase-based membranes with hierarchical porosity and photocatalytic properties. J Colloid Interf Sci 304:545–548
65. Tadros TF (1991) Steric stabilisation and flocculation by polymers. Poly J 23:683–696